Statistica Sinica Preprint No: SS-2022-0029	
Title	An Extreme-value Test for Structural Breaks in Spatial Trends
Manuscript ID	SS-2022-0029
URL	http://www.stat.sinica.edu.tw/statistica/
DOI	10.5705/ss.202022.0029
Complete List of Authors	Chenyu Han, Ngai Hang Chan and Chun Yip Yau
Corresponding Authors	Ngai Hang Chan
E-mails	nhchan@cityu.edu.hk

Statistica Sinica: Preprint
doi:10.5705/ss.202022.0029

An Extreme-Value Test for Structural Breaks in Spatial Trends

Chenyu HAN[1], Ngai Hang CHAN[2] and Chun Yip YAU[1]

[1] *The Chinese University of Hong Kong*

[2] *City University of Hong Kong*

Abstract:

Non-stationary spatial phenomena are common in various fields such as climate and medical image processing. While many methods examine non-stationary spatial covariance structures, more methods are needed for detecting sudden trend breaks in spatial data. Based on the maximal value of the neighboring discrepancy measurement in the sample space, this paper presents an extreme-value test statistic to detect trend breaks. A simulation-based algorithm is developed to detect breaks in spatial trends at various locations, from which the shape of changing boundaries can be revealed. A simulation study reveals that the test is very effective in detecting structural breaks, especially when they appear at the boundary of the sampling region. Analyses of Australian rainfall and lung tumor data demonstrate the accuracy and wide applicability of the proposed method.

Key words and phrases: change boundary, extreme value theory, inference, long-run variance.

Statistica Sinica: Preprint
doi:10.5705/ss.202022.0029

1. Introduction

Non-stationary spatial phenomena are commonly detected in biological, environmental and geographical fields. Non-stationarity can occur in both spatial trends and covariance structures. While many studies have examined non-stationary covariance structures, non-stationarity in the spatial trends needs more attention. One of the most popular methods for the inference of spatial trends is kriging, as discussed by Cressie (1993). However, when little is known about the covariance structure of the data, kriging may not be effective. Furthermore, many kriging methods cannot accurately detect a sudden change in trends, such as those reported by Jun and Stein (2008) for air pollution, Sherwood (2007) for climate change modeling, Neill (2012) for infectious disease patterns, and Otto and Schmid (2016) for computer tomography scans of tumors. It is essential to detect not only structural breaks, but also specific spatial patterns in the underlying spatial trend to avoid misspecifications of spatial models.

Specifically, assume that the data are described by the following spatial model:

$$Y(\mathbf{s}) = \mu(\mathbf{s}) + \epsilon(\mathbf{s}),$$

where $\mathbf{s}$ denotes a location in the sample space. That is, the data Y at point

Statistica Sinica: Preprint
doi:10.5705/ss.202022.0029

$\mathbf{s}$ is composed of the underlying trend μ and the zero-mean error term ϵ. Without loss of generality, we assume that the dimension of the sample space is 2. We also assume that the data are observed regularly on a grid. Thus, the spatial model can be specified as

$$Y(\mathbf{i}) = \mu(\mathbf{i}/\mathbf{n}) + \epsilon_{\mathbf{i}}\,, \tag{1.1}$$

where $\mathbf{i} = (i_1, i_2) \in \{1, \ldots, n_1\} \times \{1, \ldots, n_2\}$ is the location vector in a 2-dimensional sample space, $\mathbf{n} = (n_1, n_2)$, with each n_j denoting the sample size of the j-th dimension, $j = 1, 2$, and $\mathbf{i}/\mathbf{n} = (i_1/n_1, i_2/n_2)$. Assume that the error term $\epsilon_{\mathbf{i}}$ can be expressed as a function of an i.i.d. spatially random process $\eta_{\mathbf{i}}$, that is, $\epsilon_{\mathbf{i}} = g(\eta_{\mathbf{i}-\mathbf{j}}, j \in Z^2)$, where Z is the set of integers. A typical error process is the spatial linear process $\epsilon_{\mathbf{i}} = \sum_{\mathbf{j}\in Z^2} \alpha(\mathbf{i}-\mathbf{j})\eta_{\mathbf{j}}$ that has been studied in Hallin et al. (2001) and Lahiri and Robinson (2016), where $\{\eta_{\mathbf{j}}\}$ is a collection of independent zero mean random variables with a common variance 1. In model (1.1), the sampling structure is the infill asymptotics given in Cressie (1993), in which the sample space is fixed and the distance between the neighboring samples tends to zero.

Assume that the trend function $\mu(\cdot)$ is piecewise Hölder continuous on the region $I = [0, 1]^2 \subset \mathbb{R}^2$. If this function does not satisfy the Hölder continuity condition in any neighbors of a point $\mathbf{s} \in I$, then such a point is considered as a structural break point. Accordingly, the following topics

Statistica Sinica: Preprint
doi:10.5705/ss.202022.0029

are pursued in this paper.

1. We determine whether a trend has no structural breaks on I, that is, H_0: the trend function $\mu(\cdot)$ is α-order Hölder continuous on the region $I = [0,1]^2 \subset \mathbb{R}^2$, which is written as

$$H_0 : \ \mu(\cdot) \in H^{\alpha}(I).$$

2. If the null hypothesis H_0 is rejected, i.e., structural breaks exist, then there exists at least one subset B of I, such that $\min_{\mathbf{i}\in B,\mathbf{j}\in B^c} |\mu(\mathbf{i}) - \mu(\mathbf{j})| \geq C$ for some constant $C > 0$. We aim to detect all possible changing boundaries in the region I that partition I into disjoint subsets B_i, such that the trend $\mu(\cdot)$ is Hölder continuous in each B_i but not in two adjacent regions $B_i \cup B_j$, $i \neq j$. Therefore, the changing boundary can be expressed as ∂B_i.

Before modelling the structural breaks in the trend, we identify the source of variability by examining some of the structural assumptions of the error. As Tang and MacNeill (1993) noted, statistical properties of change-point estimates can be significantly affected by the presence of serial correlations. We follow the approach of Wu (2007) and Wu and Zhao (2007) for the one-dimensional case and that of El Machkouri et al. (2013) for the higher-dimensional cases to identify the variability in a trend from its error

Statistica Sinica: Preprint
doi:10.5705/ss.202022.0029

structure. To this end, for a given zero-mean stationary error process $\epsilon_{\mathbf{i}} = g(\eta_{\mathbf{i}-\mathbf{j}}, j \in Z^2)$, where $\eta_{\mathbf{i}}$ are i.i.d. random variables and g is a measurable function, denote an i.i.d. copy of $\eta_{\mathbf{i}}$ by $\eta'_{\mathbf{i}}$, and define

$$\eta^*_{\mathbf{i}} = \begin{cases} \eta_{\mathbf{i}}, & \text{if } \mathbf{i} \neq 0\,, \\ \eta'_{\mathbf{i}}, & \text{if } \mathbf{i} = 0\,, \end{cases}$$

with $\epsilon^*_{\mathbf{i}} = g(\eta^*_{\mathbf{i}-\mathbf{j}}, j \in Z^2)$. Then, the physical dependence measure for the L_p random variable $\epsilon_{\mathbf{i}}$ is given by

$$\delta_{\mathbf{i},p} = || \epsilon_{\mathbf{i}} - \epsilon^*_{\mathbf{i}} ||_p\,,$$

where $|| \cdot ||_p$ is the L_p norm. Let $S_{\Gamma_n} = \sum_{\mathbf{i}\in\Gamma_n} \epsilon_{\mathbf{i}}$, where the region Γ_n satisfies $|\ \Gamma_n\ | \to \infty$ and $|\partial\Gamma_n|/|\Gamma_n| \to 0$, with $|\ \Gamma_n\ |$ denoting the cardinality of Γ_n, and $\partial\Gamma_n$ denoting the boundary of Γ_n. If $\Delta_2 = \sum_{\mathbf{i}\in Z^2} \delta_{\mathbf{i},2} < \infty$, then the normalised summation of the stationary process $\epsilon_{\mathbf{i}}$ in a region Γ_n, i.e., $S_{\Gamma_n}/\sqrt{|\ \Gamma_n\ |}$, converges to a normal distribution with a mean of zero and variance $\sigma^2 = \sum_{\mathbf{k}\in Z^2} E(\epsilon_{\mathbf{0}}\epsilon_{\mathbf{k}})$, which is known as the spatial long-run variance, see El Machkouri et al. (2013). Moreover, we can approximate the error process $\epsilon_{\mathbf{i}}$ with $\sigma Z_{\mathbf{i}}$, which is the spatial long-run standard deviation times an i.i.d. standard normal random process. We assume that the error process satisfies all of the necessary conditions for a normal approximation, that is, $\Delta_2 < \infty$. An important task here is to estimate σ.

Statistica Sinica: Preprint
doi:10.5705/ss.202022.0029

The remainder of this paper is organized as follows. Section 2 discusses existing methods for detecting breaks in trends, and then presents an extreme-value type test statistic for detecting breaks in spatial trends and examines its asymptotic distribution and power under some appropriate conditions. Section 3 devises two long-run variance estimators for the error term. Section 4 introduces a Monte Carlo-based algorithm to perform boundary-change detection. Section 5 details simulations and real data analyses that demonstrate the efficiency and advantages of our methods. Section 6 concludes and proposes some directions for future research. Proofs of the theorems are given in the Supplementary Material.

2. Extreme-Value Test Statistics

2.1 Review of Existing Methods

Many studies have been devoted to detecting the structural breaks for $d = 1$, that is, in a time series context. For independent error terms, Müller (1992) and Wu and Chu (1993) proposed test statistics based on kernel-type smoothers, while Spokoiny (1998) used a local polynomial estimator with adaptive windows. Similarly, for dependent error terms, various methods have been developed; see Robinson (1997), Davis et al. (2006) and Chan et al. (2014). In particular, for situations where the dependence between Y_i

Statistica Sinica: Preprint
doi:10.5705/ss.202022.0029

and Y_j is described by their distance $|i-j|$, Wu and Zhao (2007) devised two versions of maximum absolute deviation statistics based on the blocking technique to test for $H_0 : \mu(\cdot) \in H^1(I)$. They proved that the maximum test statistic converges to a Gumbel distribution under certain regularity conditions.

When the spatial dimension $d \geq 2$, changes can occur in a spatial fashion so the situation is more complicated. For such situations, methods such as subset scanning in Kulldorff (2001) and Neill (2012), and the likelihood ratio test for searching of the changing circle with a radius from an origin (Otto and Schmid (2016)), have been proposed. However, these methods suffer from different drawbacks. Subset scanning requires checking all of the possible subsets of the data, meaning that up to 2^n scans are needed for a sample size of n. The likelihood ratio test requires the error terms to be Gaussian with no spatial dependence structure, and is inapplicable when more than two changes occur in different places.

Recently, Chan et al. (2022) use an Integrated Squared Error (ISE) test statistic G_n to derive a test for structural changes based on the sample means of several local discrepancy measurements. Specifically, with a sample of size $n = n_1 n_2$ observed in n_1 rows and n_2 columns, several local windows of size $2k_n \times 2k_n$ are employed to scan and detect changes in different

Statistica Sinica: Preprint
doi:10.5705/ss.202022.0029

parts of the data. The local windows are centered at $(x_i, y_j) := (ik_n, jk_n)$ for $i = 1, \ldots, m_1 = [n_1/k_n]$ and $j = 1, \ldots, m_2 = [n_2/k_n]$, and they measure the local discrepancy around the point (x_i, y_i) by

$$T_n(x_i, y_j) = \sum_{l=1}^{4} \{S_l(x_i, y_j) - S_{l+1}(x_i, y_j)\}^2 , \tag{2.1}$$

where $S_l(x_i, y_j) = \frac{1}{k_n^2} \sum_{(p,q)\in D_l(x_i,y_j)} Y(p, q)$, $l = 1, ..., 4$, are respectively the sample mean of observations on the sized $k_n \times k_n$ blocks,

$$\begin{aligned} D_1(x_i, y_j) &= [x_i, x_i + k_n) \times [y_j, y_j + k_n) , \; D_2(x_i, y_j) = [x_i - k_n, x_i) \times [y_j, y_j + k_n) , \\ D_3(x_i, y_j) &= [x_i - k_n, x_i) \times [y_j - k_n, y_j) , \; D_4(x_i, y_j) = [x_i, x_i + k_n) \times [y_j - k_n, y_j) , \end{aligned}$$

in the four quadrants originating from (x_i, y_j), and $S_5(x_i, y_j) = S_1(x_i, y_j)$; see Figure 1 for an illustration. Note that there are in total $m_1 \times m_2$ local windows and they are overlapping. The test statistic which combines all local discrepancies is defined by

$$G_n = \frac{k_n^2}{n} \sum_{i=0}^{m_1} \sum_{j=0}^{m_2} T_n(x_i, y_j) . \tag{2.2}$$

Clearly, a large value of G_n indicates large discrepancies between spatial regions, and thus favors the alternative hypothesis that structure breaks exist.

Statistica Sinica: Preprint
doi:10.5705/ss.202022.0029

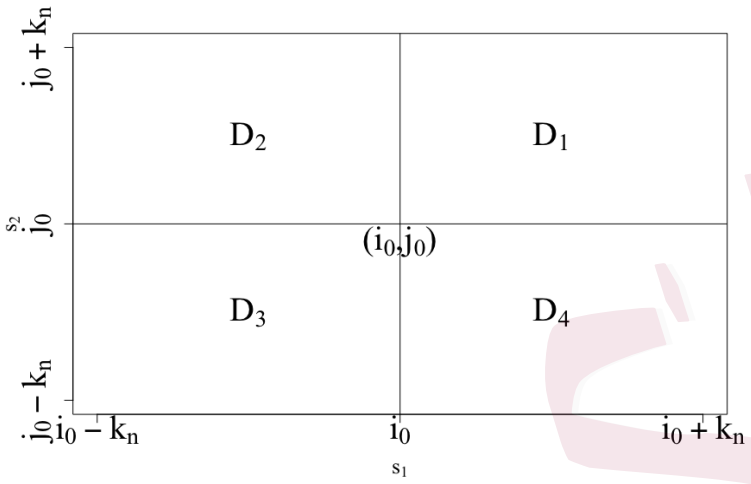

Figure 1: Blocks $D_l(i_0, j_0)$, $l = 1, \ldots, 4$, for a point (i_0, j_0).

2.2 Extreme-Value Test Statistics

Although the ISE test statistic is useful for testing structural breaks, it has some drawbacks. Many applications suffer from the limitation of physical constraints in the sense that when a structural break in spatial trends occurs near the edge of the sampling region, there may not be enough data points on both sides of the change boundary (see the Australian rainfall example in Section 5.4). In such cases, the ISE method mostly captures local discrepancies in the region where no structural breaks occur. Thus, the pattern of actual structural breaks is difficult to detect. On the other hand, observe that the discrepancy measurements $\{T_n\}$ for a stationary pro-

Statistica Sinica: Preprint
doi:10.5705/ss.202022.0029

cess and that for a piecewise stationary process are different mainly at the extremes. This is because the extremely large discrepancy measurements mainly come from the neighbors of the change points which constitute a small proportion of the spatial points. We therefore devise a test statistic based on the extremal observations as

$$\hat{G}_n = \max_{1\le i\le m_1; 1\le j\le m_2} T_n(x_i, y_j)\,. \tag{2.3}$$

By using extreme value theory and the strong invariance principle, the following theorem asserts that the extreme-value statistic $\hat{G}_n$ converges to a Gumbel distribution after a proper normalization.

Theorem 1.

i. Suppose that $\mu(\cdot) \in H^{\alpha}(I)$.

(a) If the error process $\{\epsilon_{\mathbf{i}}\}$ *satisfies* $\Delta_4 < \infty$, $||\ \epsilon_{\mathbf{i}} - \epsilon^*_{\mathbf{i}}\ ||_4 = O(n^{-1}(i_1 i_2)^{-2})$ *for* $\mathbf{i} = (i_1, i_2) \in Z^2$, *and*

$$k_n^{(1+\alpha)} / \min(n_1, n_2)^{\alpha} + k_n^{-1} n^{1/4} \log n \to 0\,, \tag{2.4}$$

as $n, n_1, n_2 \to \infty$, *then*

$$(k_n^2 \hat{G}_n/\sigma^2 - d_m)/6 \to_d \Lambda\,, \tag{2.5}$$

where $\sigma^2 = \sum_{\mathbf{k}\in Z^2} E(\epsilon_{\mathbf{0}}\epsilon_{\mathbf{k}})$ *is the spatial long-run variance,* $d_n = 6[\log n + \frac{1}{3}\log(\log n) - \log\Gamma(4/3)]$, Λ *is a standard Gumbel distri-*

Statistica Sinica: Preprint
doi:10.5705/ss.202022.0029

bution with distribution function $\Lambda(x) = \exp(-e^{-x})$ *and* $\Gamma(x) = \int_0^\infty t^{x-1}e^{-t}\,dt$ *is the Gamma function.*

(b) *If the error is a linear process* $\epsilon_{\mathbf{i}} = \sum_{\mathbf{j}\in Z^2} \alpha(\mathbf{i}-\mathbf{j})\eta_{\mathbf{j}}$ *satisfying* $\sum_{\mathbf{j}\in Z^2} \alpha(\mathbf{i}-\mathbf{j})^2 < \infty$ *and* $\alpha(\mathbf{i}-\mathbf{j}) = O(n^{-1}e^{-\max(|j_1|,|j_2|)})$, $\eta_{\mathbf{i}} \in L^q$, $q > 4$, *and*

$$k_n^{(1+\alpha)}/\min(n_1,n_2)^\alpha + k_n^{-1}n^{1/q} \to 0\,, \tag{2.6}$$

as $n, n_1, n_2 \to \infty$, *then* (2.5) *holds.*

ii. If there exists a constant $C > 0$ *and a subset* B *of* $I = [0,1]^2$ *with a positive Lebesgue measure such that* $\min_{x\in B, y\in B^c} |\mu(x) - \mu(y)| \geq C$, *and* (2.4) *holds, then the power of the extreme-value test approaches* 1 *as* $n, n_1, n_2 \to \infty$.

Remark 1. Theorem 1(i) provides two sets of conditions that give the convergence result (2.5). In both of the conditions (2.4) and (2.6), the first term indicates that the block length k_n should be small enough to ensure that the differences between several approximated values of Brownian motions are controlled, whereas the second term indicates that k_n should be large enough so that the Brownian motion approximation in a single block is valid. See Wu and Zhao (2007) for similar conditions in time series context. Theorem 1i(a) imposes weaker dependence assumptions, and a proper

Statistica Sinica: Preprint
doi:10.5705/ss.202022.0029

choice of k_n exists only when the Hölder exponent $\alpha > 1$. That is, if the trend is a constant. For example, when $n_1 = n_2 = \sqrt{n}$ and $\alpha = 2.1$, one possible choice of k_n is $An^{1/3}$ for some $A > 0$. In Theorem 1i(b), the specific assumption of linear error process allows an optimal k_n to be determined when $\alpha \leq 1$. In Section 5, several simulations and data analyses show that the test is effective when $k_n = An^{1/3}$ with A ranges in $[0.2, 0.4]$.

Remark 2. For the power analysis in Theorem 1 ii), the jump size C can be relaxed as C_n which depends on the sample size n. In particular, the arguments in the proof remain valid for $\log n = o(nC_n^2)$. That is, even if the break size $C_n \to 0$ as $n \to \infty$, the power of the test can still approach 1.

Remark 3. The block lengths in the two dimensions can be taken to be different, say $k_{n,1}$ and $k_{n,2}$, to allow for different sampling rates in each dimension. By similar approaches given in the proofs of the Supplementary Materials, we can show that when

$$k_{n,1}^{\alpha+1/2} k_{n,2}^{1/2} n_1^{-\alpha} + k_{n,2}^{\alpha+1/2} k_{n,1}^{1/2} n_2^{-\alpha} + (k_{n,1} k_{n,2})^{-1/2} n^{1/4} \log n \to 0\,, \qquad (2.7)$$

holds as $n, n_1, n_2 \to \infty$, then

$$(k_{n,1} k_{n,2} \hat{G}_n / \sigma^2 - d_{m'})/6 \to_d \Lambda\,,$$

Statistica Sinica: Preprint
doi:10.5705/ss.202022.0029

where $m' = [\frac{n}{k_{n,1}k_{n,2}}]$, and σ, d_n, Λ are defined in Theorem 1. Similarly, under the local alternative with a jump size C_n, the power of the test approaches 1 if $\log n = o(nC_n^2)$ and (2.7) holds.

3. Long-Run Variance Estimator

Use of the extreme-value statistics requires an adequate estimate of the spatial long-run variance $\sigma^2 = \sum_{\mathbf{k}\in Z^2} E(\epsilon_{\mathbf{0}}\epsilon_{\mathbf{k}})$, where $\epsilon_{\mathbf{i}}$s are the underlying zero-mean error terms. Several methods have been presented when the spatial dimension is one, see Herrmann et al. (1992) and Hall et al. (1990). In addition, a bootstrap method was proposed by Bühlmann (2002) and a subsampling method was introduced in Politis et al. (1999). More recently, Wu and Zhao (2007) applied a blocking method to devise several estimators for the one-dimensional long-run variance when the trend function μ is Lipschitz continuous. Some of these methods also exhibit good consistency when μ has multiple structural breaks.

Following the blocking approach, we devise two spatial long-run variance estimators based on the mean and the median of the local discrepancy measurements respectively as follows:

$$\hat{\sigma}_1^2 = \frac{k_n^2}{8(m_1-1)(m_2-1)} \sum_{i=1}^{m_1-1} \sum_{j=1}^{m_2-1} T_n(x_i, y_j)\,, \tag{3.1}$$

Statistica Sinica: Preprint
doi:10.5705/ss.202022.0029

and

$$\hat{\sigma}_2^2 = \frac{k_n^2}{M_0}\text{median}\{T_n(x_i, y_j); i = 1, \ldots, m_1, j = 1, \ldots, m_2\}\,, \tag{3.2}$$

where $M_0 \approx 6.1$ is the median of the Gamma distribution $\Gamma(4/3, 1/6)$.

We use $\hat{\sigma}_2^2$ in the following applications as it is a median of the local discrepancy and is thus more robust when one encounters large jumps in the trend μ, whereas $\hat{\sigma}_1^2$ is more vulnerable as it uses all of the data in the sampling region. In particular, under some regularity conditions, we prove the following theorem.

Theorem 2. *Under the same conditions in Theorem 1(i),* $\hat{\sigma}_2^2 \to \sigma^2$ *in probability.*

Remark 4. The long-run variance estimator also requires a choice of block length k_n. The same choice of k_n in Section 2 can be adopted. Alternatively, in our simulation studies, we find that for a fixed sample size n, the estimator of long-run variance first increases with k_n, then remains relatively stable for an interval of k_n, before finally exploding when the block length approaches the number of rows n_1 or the number of columns n_2. Thus, we can obtain an estimator $\hat{\sigma}_2^2$ of long-run variance by choosing a k_n which lies in the interval where the estimator remains stable.

Statistica Sinica: Preprint
doi:10.5705/ss.202022.0029

4. Boundary Change Detection

In many applications, we are not only interested in detecting the existence of structural breaks, but also in determining locations of the stationary regions. In this section, we introduce a method for estimating the changing boundaries based on the local discrepancy measure T_n in (2.1) when the error process $\{\epsilon_{\mathbf{i}}\}$ satisfies the assumptions given in Section 1, that is, $\Delta_2 < \infty$.

Compared with one-dimensional change point detection problems, spatial change-boundaries have many more directions, shapes and complicated dependence structures. Thus, an analytic approximation of the change-boundary seems unachievable. Alternatively, using the Monte Carlo-based hypothesis testing method of Kulldorff (1999), we develop a boundary estimation procedure as follows. The key idea is to compare the test statistic computed from the observed process with the simulated test statistics computed from random replications of a spatial white noise process which mimics the observed process. The comparison is made for each spatial point in the sampling region. Thus, adjustments for dependent multiple testings are needed to control the false discovery rate. The detected change-points are finally interpolated to constitute the estimated boundary. The detailed algorithm is described as follows.

Statistica Sinica: Preprint
doi:10.5705/ss.202022.0029

The algorithm for estimating change-boundaries

1. Generate $2k_n \times 2k_n$ i.i.d. standard normal samples $Z_{11}, ..., Z_{2k_n,2k_n}$, and compute $T_{n,Z} = \sum_{i=1}^{4}(S_{i+1,Z} - S_{i,Z})^2$, where $S_{1,Z} = \sum Z_{ij}I(i > k_n, j > k_n)$, $S_{2,Z} = \sum Z_{ij}I(i \leq k_n, j > k_n)$, $S_{3,Z} = \sum Z_{ij}I(i \leq k_n, j \leq k_n)$, $S_{4,Z} = \sum Z_{ij}I(i > k_n, j \leq k_n)$, and $S_{5,Z} = S_{1,Z}$.

2. Repeat Step 1 for r times to obtain a series of $\{T_{n,Z}\}$ to serve as the benchmark under the null hypothesis. Denote the order statistics of the series as $T_{n,Z_{(1)}} \leq ... \leq T_{n,Z_{(r)}}$.

3. Let $\hat{\sigma}^2 = \hat{\sigma}_1^2$ or $\hat{\sigma}_2^2$ be an estimator of the long-run variance σ^2 for the observed process Y as discussed in Section 3. For each of $\{(i,j); i = 1, \ldots, n_1, j = 1, \ldots, n_2\}$, compute $T_n((x_i, y_j))$ and the corresponding p-value $p_{i,j} = \frac{1}{r}\sum_{k=1}^{r} I(T_n((x_i, y_j))/\hat{\sigma}^2 < T_{n,Z_{(k)}})$. Let the order statistics of the p-values be $p_{(1)} \leq ... \leq p_{(n)}$, and denote the sample point associated with $p_{(v)}$ as (x_{i_v}, y_{j_v}).

4. Apply the adjustment given in Benjamini and Hochberg (1995) and Benjamini and Yekutieli (2001). Specifically, for $v = 1, ..., n$ and a prescribed desired false discovery rate α, if $p_{(v)} < \alpha\frac{v}{n}$, then we declare that (i_v, j_v) is a change point with a confidence level of $(1 - \alpha)$.

5. Connect all of the change points with line segments and draw the

Statistica Sinica: Preprint
doi:10.5705/ss.202022.0029

estimated change boundary.

Some examples of the use of this approach are discussed in Section 5.

5. Simulations and Data Analysis

In this section, we present simulation studies and data analyses to investigate the performance of the proposed spatial long-run variance estimator, extreme-value test, and change-boundary estimation algorithm. Moreover, two real data sets drawn from climate and medical imaging studies are analysed to demonstrate the applicability of our method. In all subsequent discussions in this section, a spatial location is generally denoted as $\mathbf{s} = (s_1, s_2)$, and the sample size is denoted as $n = n_1 n_2$, that is, the samples are distributed in n_1 rows and n_2 columns.

5.1 Estimation of Spatial Long-Run Variance

First, we investigate the performance of the spatial long-run variance estimators. We consider the following four error processes $\{\epsilon_{ij}\}$ that are generated from a standard normal white noise process $\{\eta_{ij}\}$.

1. An i.i.d. error process: $\epsilon_{ij} = \eta_{ij}$;

2. A weakly dependent spatial AR (1,1) process: $\epsilon_{ij} = 0.1\epsilon_{i-1,j} + 0.2\epsilon_{i,j-1} + 0.1\epsilon_{i-1,j-1} + \sqrt{1 - 0.4^2}\eta_{ij}$;

Statistica Sinica: Preprint
doi:10.5705/ss.202022.0029

3. A strongly dependent spatial AR(1,1) process: $\epsilon_{ij} = 0.3\epsilon_{i-1,j}+0.2\epsilon_{i,j-1}+ 0.3\epsilon_{i-1,j-1} + \sqrt{1-0.8^2}\eta_{ij}$.

4. A negatively dependent spatial AR (1,1) process: $\epsilon_{ij} = -0.1\epsilon_{i-1,j} - 0.2\epsilon_{i,j-1} - 0.1\epsilon_{i-1,j-1} + \sqrt{1-0.4^2}\eta_{ij}$;

As the sum of the absolute values of the coefficients of the AR terms is less than 1, these four processes are stationary. However, the third process has a stronger dependence and is closer to nonstationarity since the sum of the absolute values of the coefficients is closer to 1.

We apply $\hat{\sigma}_1^2$ and $\hat{\sigma}_2^2$ to estimate the long-run variance of each of the process under sample size $n_1 = n_2 = 900$ and 100 replications. The block length is taken as $k_n = 0.2n^{1/3} \approx 18$. The means and standard deviations of the estimated long-run variances are reported in Table 1. It can be seen that the two methods have similar performance.

5.2 Testing for Structural Breaks: Different Locations

Here, we apply our extreme-value test statistic (2.2), termed as "Max SE" herein, to test the hypothesis: $H_0 : \mu(\mathbf{s}) = 0$ versus $H_1 : \mu(\mathbf{s}) = j \cdot I(\mathbf{s} \in R)$, where j is the jump size, $I(\cdot)$ is the indicator function, and R is a spatial region. We consider two types of structural breaks of the mean function that appear in different locations in the sampling region, namely,

Statistica Sinica: Preprint
doi:10.5705/ss.202022.0029

Table 1: Estimated long-run variance value.

Estimator	$\hat{\sigma}_1^2$		$\hat{\sigma}_2^2$	
error type	mean	s.d.	mean	s.d.
i.i.d. error	1.002	0.028	0.999	0.033
Weakly dependent error	2.089	0.061	2.139	0.079
Strongly dependent error	5.696	0.145	5.885	0.162
Negatively dependent error	0.446	0.013	0.455	0.014

1. a center-jump: $\mu(\mathbf{s}) = j \cdot I(1/3 < s_1, s_2 < 2/3)$; and

2. an edge-jump: $\mu(\mathbf{s}) = j \cdot I(s_1, s_2 \geq 122/125)$,

where $\mathbf{s} = (s_1, s_2)$, $s_1, s_2 \in [0, 1]$. In the center-jump case, the structural breaks appear in a large area in the center, whereas in the edge-jump case, the structural breaks appear in a small area near the edge of the sampling region. The error processes are the four types given in Section 5.1.

As indicated in Wu and Zhao (2007), the extreme-value-type convergence is slow and it needs a large sample size n to reach an accurate approximation. As an alternative, by employing the idea of the strong invariance principle given in Wu (2007) and El Machkouri et al. (2013), we apply the

Statistica Sinica: Preprint
doi:10.5705/ss.202022.0029

following Monte-Carlo simulation steps to conduct the test:

- Generate $n = n_1 n_2$ i.i.d. samples $Z_{11}, ..., Z_{n_1 n_2}$ from the standard normal distribution, and obtain $\hat{G}_{n,Z}$ using (2.2) with the pre-specified block length k_n. Repeat the process 10^4 times to obtain the critical value defined as the empirical quantile $CV = q_{0.95}(\hat{G}_{n,Z})$ with significant level 0.95.

- Compute the $\hat{G}_n$ for the observed spatial process $Y(\mathbf{s})$, and reject the null hypothesis if $\hat{G}_n/\sigma^2 > CV$.

Besides the proposed extreme-value test, we perform the ISE test in Chan et al. (2022) as a benchmark. For each test, the significant level is set to be 0.05, and 1000 replications are performed. Also, the block length k_n is set as $0.4\sqrt[3]{n_1 n_2}$. Table 2 reports the sizes (false rejection ratios) of the ISE test and the extreme-value test under the null hypothesis for sample sizes $(n_1, n_2) = (125,125)$ and $(250,250)$, under different error processes. Observe that the false positive rates of ISE and Max SE tests using the Monte Carlo approach are similar in different cases. We can also see that strong positive dependent errors yield a smaller test size, and negative dependent errors yield a larger false discovery rate. Meanwhile, the extreme-value asymptotic approach does not perform well when the sample size is small.

Statistica Sinica: Preprint
doi:10.5705/ss.202022.0029

Table 2: Test size of ISE and Max SE test under different error structures and sample sizes.

Sample size (n_1,n_2)	(125,125)			(250,250)		
Test / Error type	ISE	Max SE (MC)	Max SE (Asym.)	ISE	Max SE (MC)	Max SE (Asym.)
i.i.d.	0.049	0.050	0.031	0.054	0.053	0.034
Weakly dependent	0.040	0.042	0.058	0.047	0.046	0.054
Strongly dependent	0.035	0.028	0.013	0.043	0.032	0.040
Negatively dependent	0.082	0.067	0.100	0.058	0.057	0.078

Statistica Sinica: Preprint
doi:10.5705/ss.202022.0029

Next, Figure 2 presents the power of the test against jump sizes in the edge-jump cases. Figure 3 presents the power of the test against jump sizes in the center-jump cases with sample size $(n_1, n_2) = (250, 250)$. The results for the center-jump cases with sample size $(n_1, n_2) = (125, 125)$ do not contain much new information and thus are reported in Section S2 of the Supplementary Material.

The results show that the extreme-value test and the ISE test are both effective when a break region is large and located at the center of the sampling region. The extreme-value test statistic, however, is much more effective than the ISE test statistic when structural breaks occur in a small area near the boundary of the sampling region.

Moreover, the effectiveness of the extreme-value test statistic increases as the sample size increases because the invariance principle approximation becomes more accurate. Observe also that the stronger dependence of the error structure has an undesirable effect on the test. In particular, the rejection threshold, which equals $q_{0.95}(\hat{G}_{n,Z}) \cdot \sigma^2$, is much higher than that in the i.i.d. and weak-dependence cases. Hence, the jump of the trend needs to be large enough to be detectable. From the perspective of test size, we draw similar conclusions: the size is accurate in the i.i.d., and weak-dependence cases but decays in the strong-dependence error cases.

Statistica Sinica: Preprint
doi:10.5705/ss.202022.0029

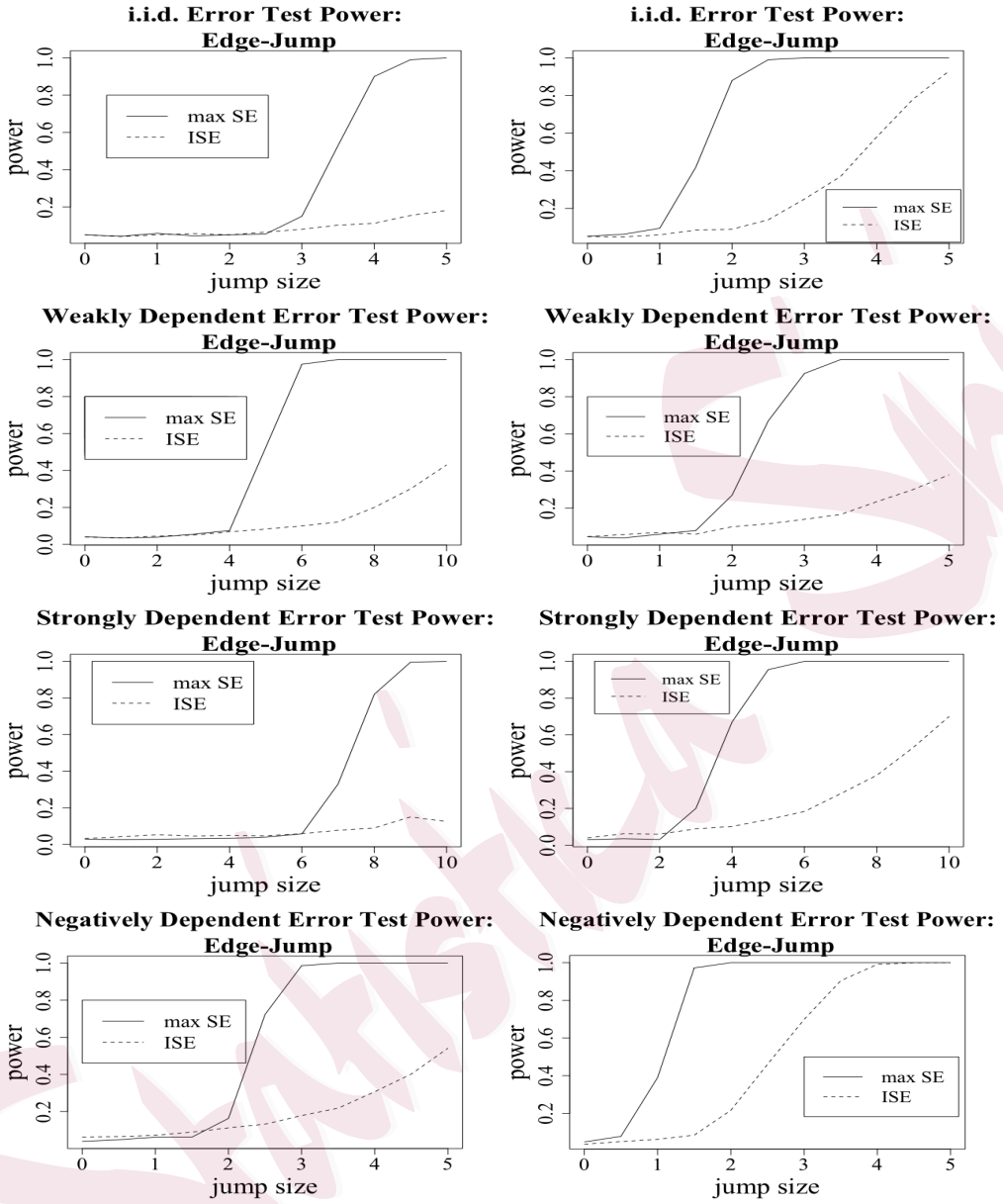

(a) Sample size $(n_1, n_2) = (125, 125)$. (b) Sample size $(n_1, n_2) = (250, 250)$.

Figure 2: Test power against jump size for the i.i.d., weakly dependent, strongly dependent and negatively dependent error term, edge-jump case.

Statistica Sinica: Preprint
doi:10.5705/ss.202022.0029

Furthermore, there is a slight tradeoff between the extreme-value test and the ISE test, as the latter can detect small jumps in a large central area more efficiently than the former (Figure 3). Nevertheless, compared with the superiority of the extreme-value test statistic in the edge-jump cases (Figure 2), the advantage of ISE test only exists in a narrower range of jump sizes.

We also consider the issue of the block length (k_n) selection. Figure 4 reports the power of the Max SE test with sample size 250×250 for various jump sizes, error structures, and k_n. Specifically, block lengths of k_n =10 ($\approx 0.25n^{1/3}$), 15 ($\approx 0.4n^{1/3}$) and 20 ($\approx 0.5n^{1/3}$) are explored. It can be seen that the test gives similar results when using different k_n. Nevertheless, it seems that for a larger structural break region (center-jump case), a larger k_n gives better performance, whereas for a smaller structural break region (edge-jump case), a smaller k_n gives slightly better performance.

5.3 Pointwise Detection: Identifying the Change Boundary

We consider the following example, in which the two-dimensional trend μ is set as $\mu(\mathbf{s}) = \begin{cases} 0\,, & \text{if } s_1^2 + (s_2 - 1)^2 < 1/4\,, \\ 5\,, & \text{if } s_1^2 + (s_2 - 1)^2 \geq 1/4 \text{ and } s_1 + s_2 > 1\,, \\ 10\,, & \text{otherwise}\,, \end{cases}$
see Figure 5. In this setting, the trend μ has multiple breaks, and the

Statistica Sinica: Preprint
doi:10.5705/ss.202022.0029

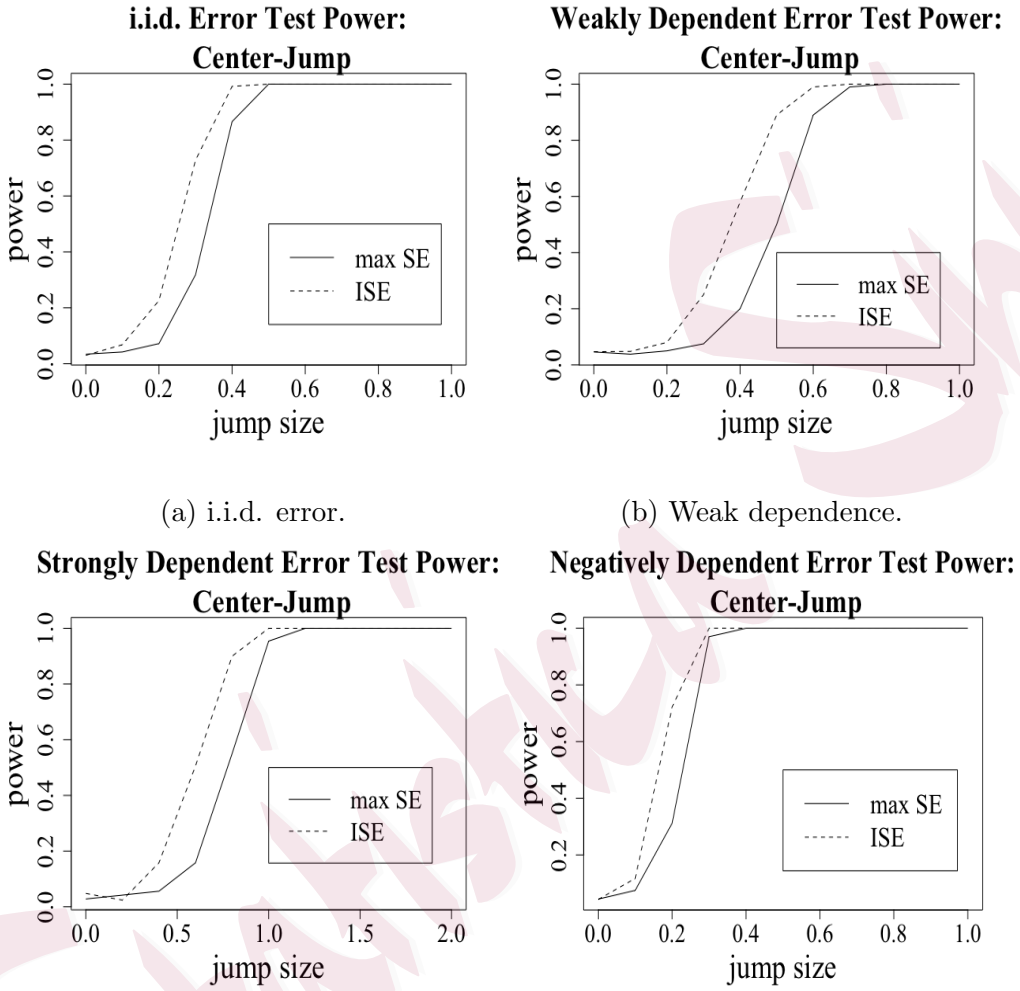

(a) i.i.d. error.

(b) Weak dependence.

(c) Strong dependence.

(d) Negative dependence.

Figure 3: Tradeoff in center-jump case.

Statistica Sinica: Preprint
doi:10.5705/ss.202022.0029

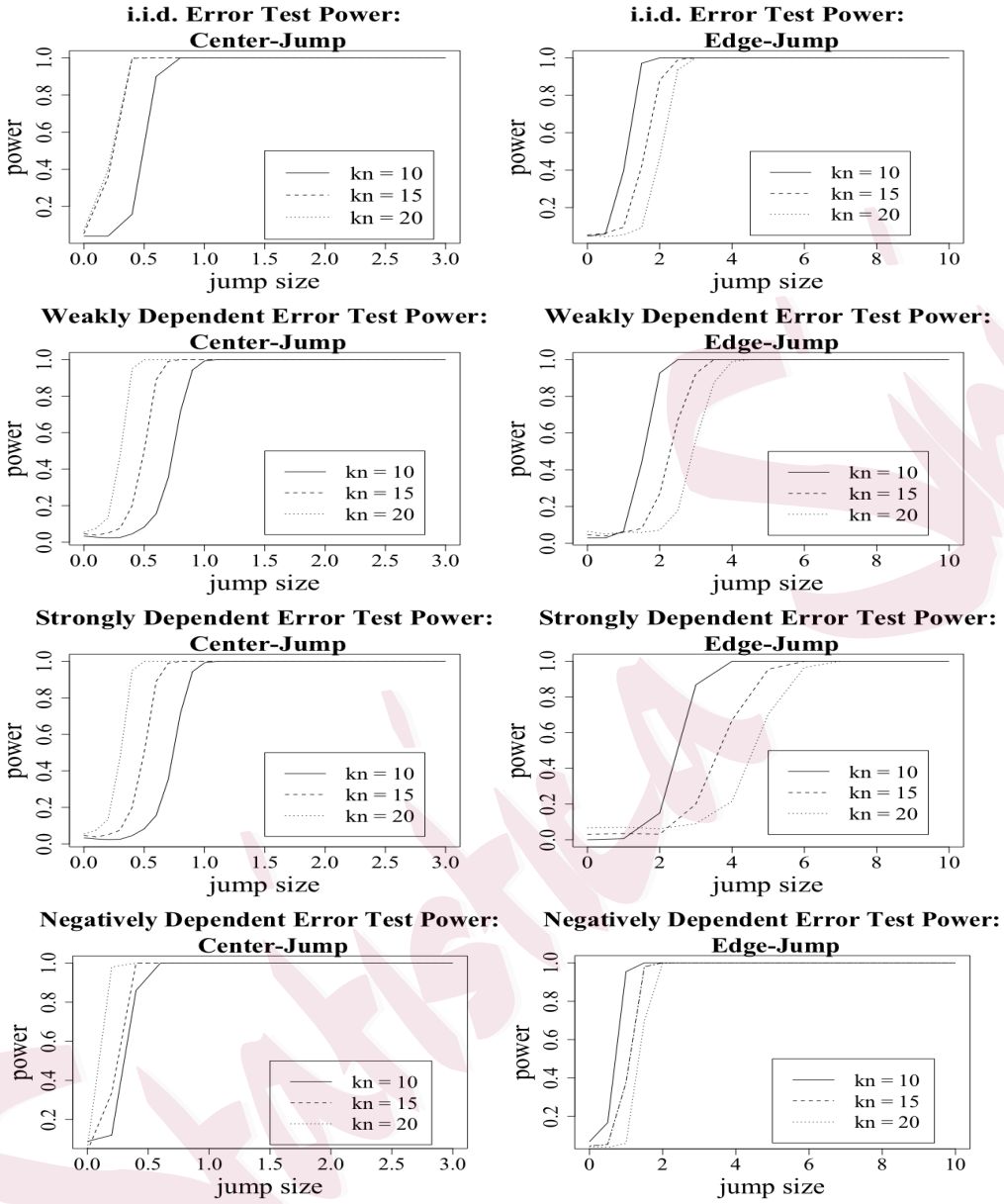

(a) Center-jump case. (b) Edge-jump case.

Figure 4: Test power against jump size for various k_n using the extreme-value test statistic.

Statistica Sinica: Preprint
doi:10.5705/ss.202022.0029

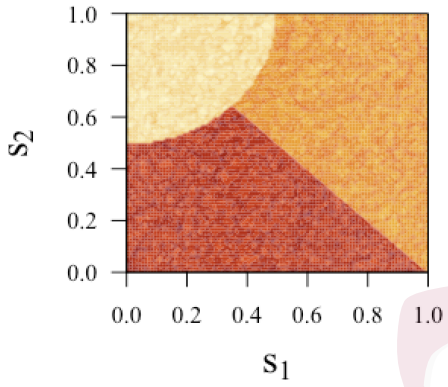

Figure 5: Actual boundary for trends $\mu(s) = 0$, $\mu(s) = 5$, and $\mu(s) = 10$.

shape of the change boundary consists of both straight lines and curves. The error term is set to be i.i.d., weakly dependent, strongly dependent or negatively dependent, as discussed above. The sample size is taken as $(n_1, n_2) = (100, 100)$, and the block length is set as $k_n = 0.2\sqrt[3]{n_1 n_2}$. Using the method presented in Section 4, we estimate the change boundary by connecting the brown points; see Figure 6. Observe that the estimated change boundaries are consistent with the true ones.

5.4 Real Data Analysis: Australian Rainfall

An example of a dataset that shows structural breaks in the edges of sampling regions is the annual rainfall data of Australia, which can be found at

Statistica Sinica: Preprint
doi:10.5705/ss.202022.0029

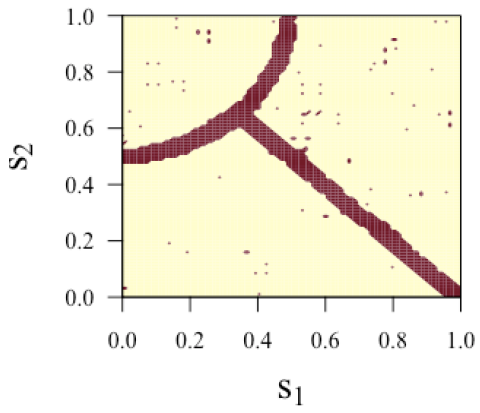

(a) i.i.d. error.

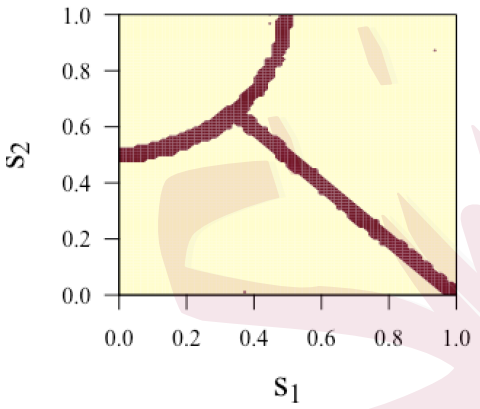

(b) Weak dependence.

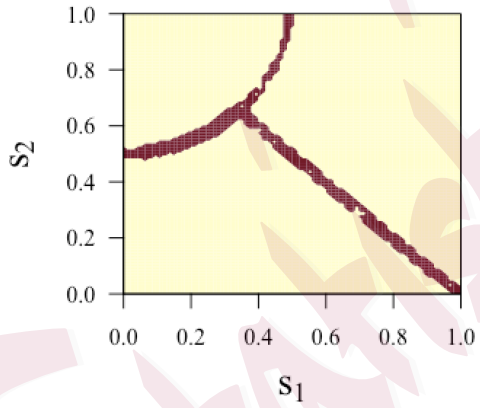

(c) Strong dependence.

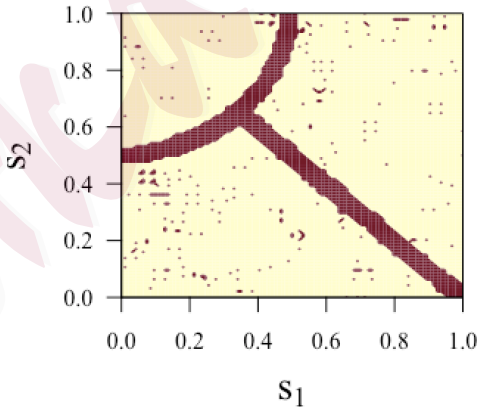

(d) Negative dependence.

Figure 6: Estimated boundary for the trends in the 0.95 confidence level.

Statistica Sinica: Preprint
doi:10.5705/ss.202022.0029

http://www.bom.gov.au/. The map in Figure 7 depicts the average annual rainfall for the period 1961 to 1990. The data takes the form of a matrix with 691 rows and 886 columns in row-major order. That is, it is written row by row starting at the northern-most row (row 1), and in each row, the data points are arranged from west to east.

Since the altitude of inland Australia is high, the moist air coming from the ocean is not able to reach the large interior part of the continent. Hence, rainfall is low in the inland but is concentrated in the small coastal areas of Australia. The structural difference in rainfall patterns between the inland and coastal areas is an obvious example of structural breaks in a spatial trend near the boundary of a sampling region.

To analyze the rainfall data, we first obtain a robust long-run variance estimate of the error structure. Specially, we standardize the data by subtracting the mean and dividing by the standard deviation, and compute the long-run variance estimator as $\hat{o}_2^2 = 73.9$. This value is relatively high since precipitation data usually has a very strong local dependence, and thus induces a large long-run variance.

Next, following the discussions in Remark 1, we conduct the Max SE and ISE tests under block lengths $k_n = [An^{1/3}]$ for several choices of A ranging from 0.25 to 0.35. For each of the Max SE and ISE methods, we

Statistica Sinica: Preprint
doi:10.5705/ss.202022.0029

Table 3: The critical values $G_{n,Z}$ and $\hat{G}_{n,Z}$, test statistics G_n and $\hat{G}_n$ under different block lengths k_n for Australian rainfall data.

Coefficient: A	0.25	0.27	0.29	0.32	0.35
Block length: k_n	21	23	25	27	30
Critical Value (ISE): $G_{n,Z}$	0.019	0.016	0.014	0.012	0.010
Critical Value (Max SE): $\hat{G}_{n,Z}$	0.191	0.162	0.131	0.111	0.089
Test Statistic (ISE): $G_n/\hat{\sigma}_2^2$	0.006	0.007	0.007	0.007	0.009
Test Statistic (Max SE): $\hat{G}_n/\hat{\sigma}_2^2$	0.236	0.216	0.211	0.260	0.141

compute the test statistic for the standardized rainfall data and employ the simulation method in Section 5.2 to obtain critical values at 99% significance level. The results are reported in Table 3. It can be seen that under all block lengths, the ISE test fails to reject the null hypothesis of no structural breaks, while the Max SE test rejects the null hypothesis and suggests the existence of structural breaks. This is in line with the findings in Section 5 that the proposed Max SE test is more effective in detecting breaks near the boundary of the spatial area.

Moreover, we apply the change-boundary estimation procedure to the data, Figure 8(a) provides a heatmap of the rainfall data and Figure 8(b)

Statistica Sinica: Preprint
doi:10.5705/ss.202022.0029

shows the estimated change boundaries. The estimated change boundaries are mainly along the east coast of Australia, which run from Cairns to Melbourne and bound the rainfall-abundant areas. In the south and southwest, the detected changes are near populated cities such as Adelaide and Perth. Indeed, these cities are the only populated areas in Southern and Western Australia because they are the only areas with adequate precipitation. In the far south, southwest and northwest, change boundaries are also detected in the sea far from the coast. These boundaries are due to an artifact in the data set that the values in those regions are all zeros.

To further justify the assumption of piecewise Hölder continuous of the spatial trends, we show that there is no trend break in each of the estimated regions using the Max SE test. Since the proposed Max SE test and all relevant tests for trend stationarity in the existing literature, up to our knowledge, focus on rectangular regions, we conduct the Max SE test on some rectangular regions which cover most of Australian inland; see the red, blue and yellow rectangular areas in Figure 8(b). Using a block length of $1/3n^{1/3}$, the values of the test statistic $\hat{G}_n/\hat{\sigma}_2^2$ and the critical values at 99% significance level are reported in Table 4. All the test statistics are smaller than the respective critical values in these cases, which implies a stationary rainfall trend in inland Australia. Moreover, observations along

Statistica Sinica: Preprint
doi:10.5705/ss.202022.0029

Table 4: The critical values $\hat{G}_{n,Z}$, test statistics $\hat{G}_n$ of different rectangle areas in Figure 8(b).

Lines of rectangle	long dashed	short dashed	dotted
Sample size: $n_1 \times n_2$	320× 670	490× 300	430×420
Block length: $1/3n^{1/3}$	20	18	19
Critical Value (Max SE): $\hat{G}_{n,Z}$	0.191	0.230	0.211
Test Statistic (Max SE): $\hat{G}_n/\hat{\sigma}_2^2$	0.066	0.025	0.126

two paths across Australia are depicted in Figures 8c) and 8d). Observe that both paths indicate continuity in the level of the observations within each estimated region, with sharp changes at the estimated boundaries.

5.5 Real Data Analysis: Lung-Tumor Computed Tomography Scans

Medical images play a significant role in diagnosis and monitoring of diseases. As it is relatively time-consuming to rely on health professionals to manually examine medical images, an automatic framework for processing medical images would be useful. A medical image can be regarded as a two-dimensional or a three-dimensional sample space of the human body.

Statistica Sinica: Preprint
doi:10.5705/ss.202022.0029

The boundary change detection algorithm is thus applicable in this context.

We consider the data reported by Otto and Schmid (2016), which consists of six left-lung computed tomography (CT) scans, presented in Figures 9 and 10. The space between each slice is 5 mm, and each slice contains 100×100 voxels, where the gap between each row and column of voxels is 0.5 mm. Each CT scan is transformed into a 100×100 matrix valued in [0,1], where the value represents the greyscale of a given voxel. When this value is higher, the voxel is lighter in color, which suggests that the passage of X-rays is blocked in this voxel. Figure 12 shows that in addition to some (physically normal) structural breaks at the edge of the scans, there is a significant tumor in Slices 2 to 5.

We aim to use our boundary-detecting algorithm to determine the location and scale of this tumor. First, for each of Slices 1–6, we apply $\hat{\sigma}_2^2$ to estimate the underlying long-run variance of the CT scans. The estimator shows consistency between different slides with the estimated long-run variances taking values around 0.01. We denote the left-bottom point of each figure as sample index (1,1), then set the block length as $0.2\sqrt[3]{n_1 n_2}$. and set the significance level as 0.99 to conduct our boundary estimation.

The brown curves in Figure 11 represent the estimated change boundaries. The shape and boundary of the tumor is clearly visible in Slices

Statistica Sinica: Preprint
doi:10.5705/ss.202022.0029

2-5. From this detected structural change, we estimate that the tumor has a diameter of ∼20 mm, and is centered at approximately (52, 43, 3.5), which is consistent with the results obtained by Otto and Schmid (2016) using likelihood estimation. Moreover, in addition to the tumor, other (normal) structural changes in the lung (e.g. the location of blood vessels and esophagus) are detected by our method, demonstrating that the proposed procedure may be a viable tool for medical diagnosis.

6. Conclusions

The extreme-valued test statistic introduced in this paper is a powerful tool for detecting structural breaks in spatial trends, as it concentrates on the largest fluctuations in sampling data and excludes interference from other non-broken areas. Using extreme value theory, we derive the asymptotic distribution for such test statistics. Moreover, we show that the spatial long-run variance estimator based on the median of the discrepancy measure can aid the use of this test, as it only requires half of the sampling region to be stable for the median of the discrepancy to remain robust. Furthermore, we develop a Monte-Carlo based algorithm and apply it to determine the shape of change boundaries. Simulations and real data analyses illustrate that these methods are widely applicable.

Statistica Sinica: Preprint
doi:10.5705/ss.202022.0029

Several important aspects: finding the optimal blocking length k_n; deriving other extreme-value type tests to deduce general conditions in asymptotic properties; and the applicability of our method for irregularly-distributed spatial data, need to be further explored. These challenging problems will be dealt with in future works.

Supplementary Material

Proofs of the main theorems and figures about the power of the test against jump sizes for the center-jump cases are presented in Supplementary Materials.

Acknowledgments

We thank the Co-Editor, an associate editor and two anonymous referees for their helpful comments and constructive suggestions. This research was supported in part by grants from HKSAR-RGC-GRF Numbers 14308218, 14307921 (Chan), and 14302423, 14302719, 14304221 (Yau).

References

Benjamini, Y. and Y. Hochberg (1995). Controlling the false discovery rate: a practical and powerful approach to multiple testing. *Journal of the Royal Statistical Society: Series B (Methodological)* *57*(1), 289–300.

Statistica Sinica: Preprint
doi:10.5705/ss.202022.0029

REFERENCES

Benjamini, Y. and D. Yekutieli (2001). The control of the false discovery rate in multiple testing under dependency. *Annals of Statistics 29*(4), 1165–1188.

Berkes, I., S. Hormann, and J. Schauer (2011). Split invariance principles for stationary processes. *The Annals of probability 39*(6), 2441–2473.

Bühlmann, P. (2002). Bootstraps for time series. *Statistical Science 17*, 52–72.

Chan, N. H., C. Y. Yau, and R.-M. Zhang (2014). Group LASSO for structural break time series. *Journal of the American Statistical Association 109*(506), 590–599.

Chan, N. H., R. Zhang, and C. Y. Yau (2022). Testing for structural breaks in spatial trends. *Statistica Sinica 32*, 1961–1981.

Chen, S. X. (2008). Nonparametric estimation of expected shortfall. *Journal of Financial Econometrics 6*(1), 87–107.

Cressie, N. (1993). *Statistics for Spatial Data*. Wiley, New York.

Davis, R. A., T. C. M. Lee, and G. A. Rodriguez-Yam (2006). Structural break estimation for nonstationary time series models. *Journal of the American Statistical Association 101*(473), 223–239.

El Machkouri, M., D. Volnỳ, and W. B. Wu (2013). A central limit theorem for stationary random fields. *Stochastic Processes and their Applications 123*(1), 1–14.

Embrechts, P., C. Klüppelberg, and T. Mikosch (2013). *Modelling Extremal Events: For Insurance and Finance*. Springer-Verlag, New York.

Statistica Sinica: Preprint
doi:10.5705/ss.202022.0029

REFERENCES

Galambos, J. (1987). *The Asymptotic Theory of Extreme Order Statistics*. Wiley, New York.

Hall, P., J. Kay, and D. Titterington (1990). Asymptotically optimal difference-based estimation of variance in nonparametric regression. *Biometrika 77*(3), 521–528.

Hallin, M., Z. Lu, and L. T. Tran (2001). Density estimation for spatial linear processes. *Bernoulli 7*(4), 657–668.

Herrmann, E., T. Gasser, and A. Kneip (1992). Choice of bandwidth for kernel regression when residuals are correlated. *Biometrika 79*(4), 783–795.

Jun, M. and M. L. Stein (2008). Nonstationary covariance models for global data. *Annals of Applied Statistics 2*(4), 1271–1289.

Komlós, J., P. Major, and G. Tusnády (1975). An approximation of partial sums of independent RV'-s, and the sample DF. I. *Zeitschrift für Wahrscheinlichkeitstheorie und Verwandte Gebiete 32*(1-2), 111–131.

Komlós, J., P. Major, and G. Tusnády (1976). An approximation of partial sums of independent rv's, and the sample df. ii. *Zeitschrift f r Wahrscheinlichkeitstheorie und Verwandte Gebiete 34*(1), 33–58.

Kotz, S. and J. W. Adams (1964). Distribution of sum of identically distributed exponentially correlated gamma-variables. *The Annals of Mathematical Statistics 35*, 277–283.

Kotz, S. and J. Neumann (1963). On the distribution of precipitation amounts for periods of increasing length. *Journal of Geophysical Research 68*(12), 3635–3640.

Statistica Sinica: Preprint
doi:10.5705/ss.202022.0029

REFERENCES

Kulldorff, M. (1999). Spatial scan statistics: models, calculations, and applications. In *Scan Statistics and Applications*, pp. 303–322. Springer.

Kulldorff, M. (2001). Prospective time periodic geographical disease surveillance using a scan statistic. *Journal of the Royal Statistical Society: Series A (Statistics in Society) 164*(1), 61–72.

Lahiri, S. and P. M. Robinson (2016). Central limit theorems for long range dependent spatial linear processes. *Bernoulli 22*(1), 345–375.

Lu, Z. and D. Tjøstheim (2014). Nonparametric estimation of probability density functions for irregularly observed spatial data. *Journal of the American Statistical Association 109*(508), 1546–1564.

Müller, H.-G. (1992). Change-points in nonparametric regression analysis. *The Annals of Statistics 20*, 737–761.

Neill, D. B. (2012). Fast subset scan for spatial pattern detection. *Journal of the Royal Statistical Society: Series B (Statistical Methodology) 74*(2), 337–360.

Otto, P. and W. Schmid (2016). Detection of spatial change points in the mean and covariances of multivariate simultaneous autoregressive models. *Biometrical Journal 58*(5), 1113–1137.

Politis, D. N., J. P. Romano, and M. Wolf (1999). *Subsampling*. Springer-Verlag, New York.

Robinson, P. M. (1997). Large-sample inference for nonparametric regression with dependent errors. *Annals of Statistics 25*(5), 2054–2083.

Statistica Sinica: Preprint
doi:10.5705/ss.202022.0029

REFERENCES

Ruymgaart, F. (2002). Sample quantiles for locally dependent processes. In *Statistical Data Analysis Based on the L1-Norm and Related Methods*, pp. 39–46. Springer-Verlag, New York.

Sherwood, S. C. (2007). Simultaneous detection of climate change and observing biases in a network with incomplete sampling. *Journal of Climate 20*(15), 4047–4062.

Spokoiny, V. G. (1998). Estimation of a function with discontinuities via local polynomial fit with an adaptive window choice. *The Annals of Statistics 26*(4), 1356–1378.

Tang, S. and I. MacNeill (1993). The effect of serial correlation on tests for parameter change at unknown time. *The Annals of Statistics 21*, 552–575.

Wu, J. and C. Chu (1993). Kernel-type estimators of jump points and values of a regression function. *The Annals of Statistics 21*(3), 1545–1566.

Wu, W. B. (2007). Strong invariance principles for dependent random variables. *The Annals of Probability 35*(6), 2294–2320.

Wu, W. B. and Z. Zhao (2007). Inference of trends in time series. *Journal of the Royal Statistical Society: Series B (Statistical Methodology) 69*(3), 391–410.

Department of Statistics, The Chinese University of Hong Kong

E-mail: hancy@link.cuhk.edu.hk

Department of Biostatistics, City University of Hong Kong

E-mail: nhchan@cityu.edu.hk

Statistica Sinica: Preprint
doi:10.5705/ss.202022.0029

REFERENCES

Department of Statistics, The Chinese University of Hong Kong

E-mail: cyyau@cuhk.edu.hk

Statistica Sinica: Preprint
doi:10.5705/ss.202022.0029

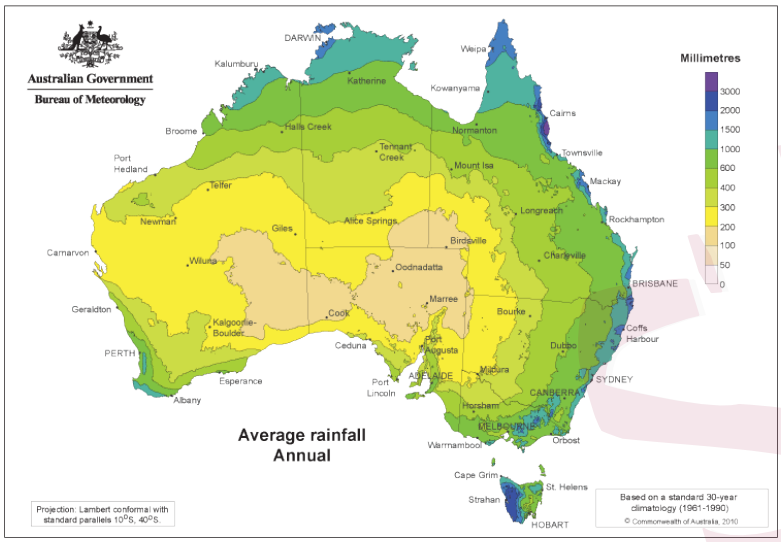

(a) Entire country.

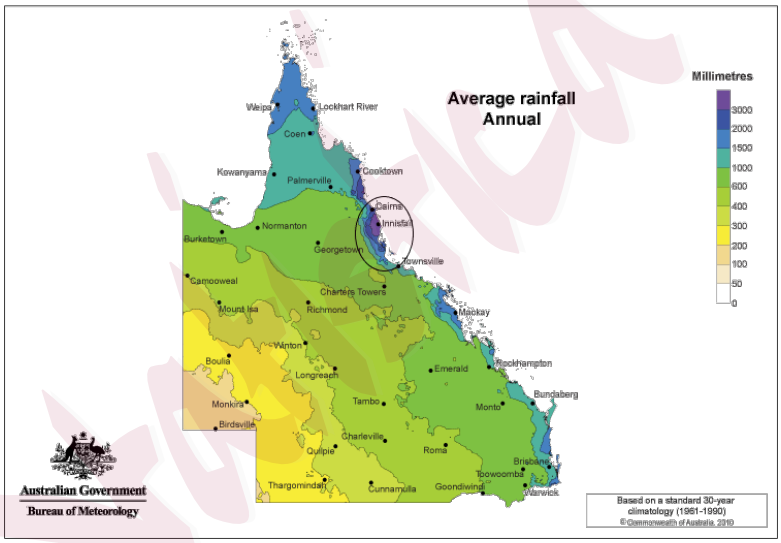

(b) Structural breaks in the edge.

Figure 7: Australian rainfall.

Statistica Sinica: Preprint
doi:10.5705/ss.202022.0029

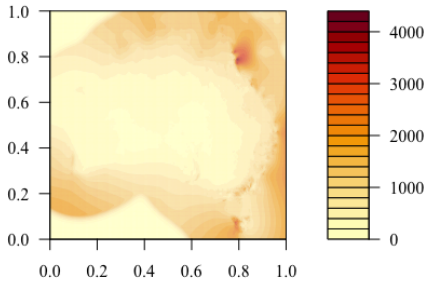

(a) Heatmap for Australian rainfall data.

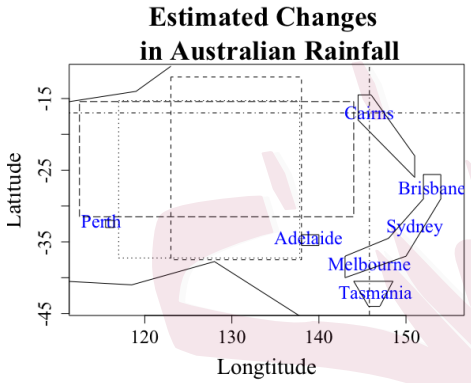

(b) Estimated change boundaries.

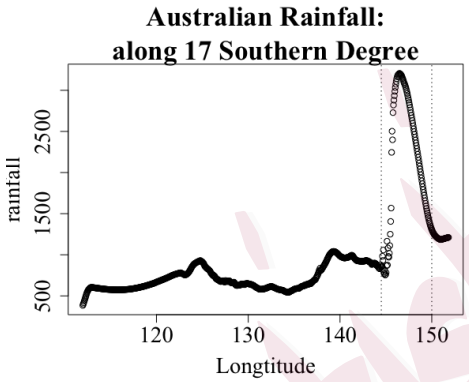

(c) Rainfall along 17°S.

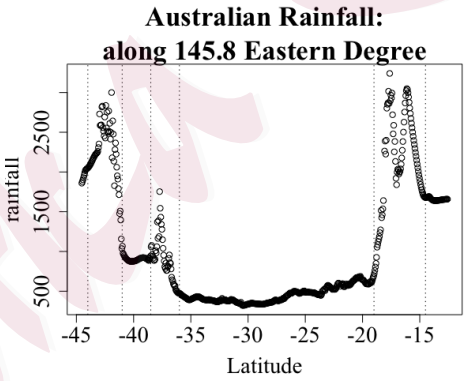

(d) Rainfall along 145°E.

Figure 8: Heatmaps, estimated change boundaries and some 1-d examples of Australian rainfall. In the heatmap (a), the left-bottom point is (45° S, 112° E) and the right-upper point is (10.5° S, 155° E).

Statistica Sinica: Preprint
doi:10.5705/ss.202022.0029

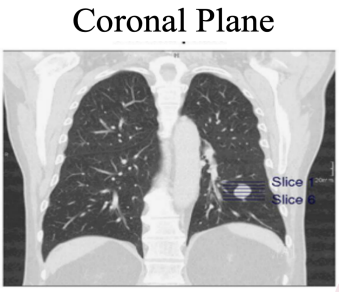

Figure 9: Location of tumor and CT slices.

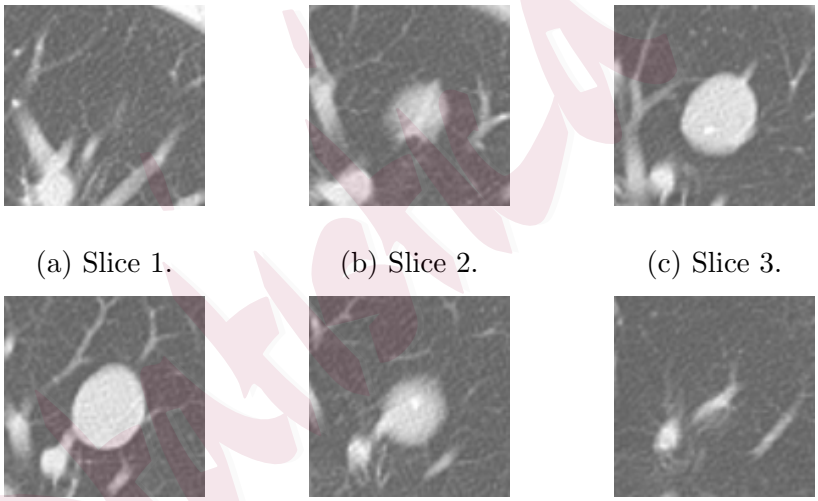

(a) Slice 1. (b) Slice 2. (c) Slice 3.

(d) Slice 4. (e) Slice 5. (f) Slice 6.

Figure 10: Lung tumor CT scans.

Statistica Sinica: Preprint
doi:10.5705/ss.202022.0029

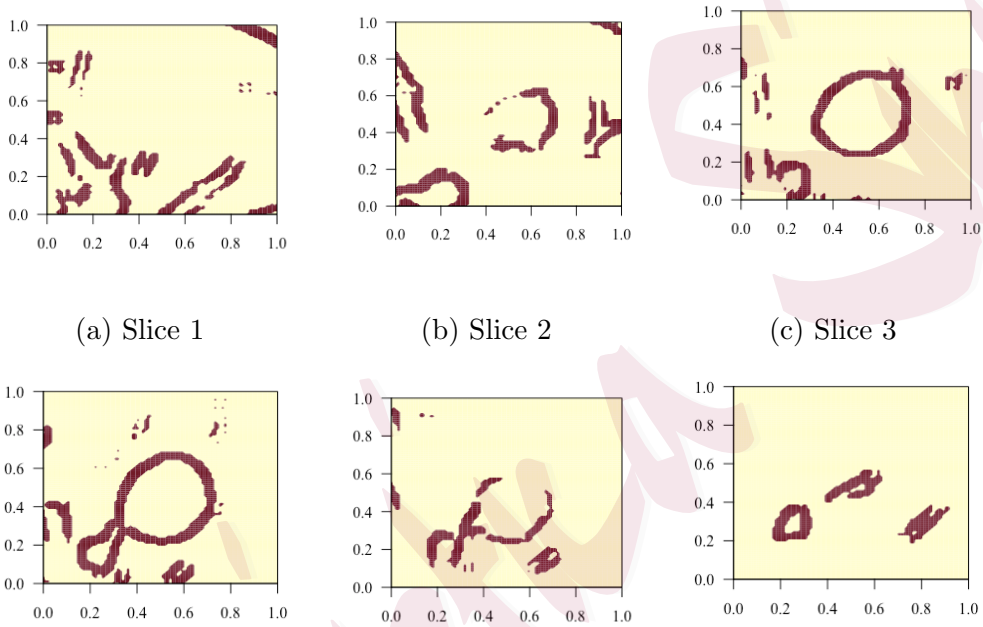

(a) Slice 1 (b) Slice 2 (c) Slice 3

(d) Slice 4 (e) Slice 5 (f) Slice 6

Figure 11: Predicted lung-tumor change boundaries.